Ferromagnetism and infrared conductivity of the homogeneous hexaboride alloy $Eu_{1-x}Ca_xB_6$

2007 J. Phys.: Condens. Matter 19 106203

(http://iopscience.iop.org/0953-8984/19/10/106203)

IOP PUBLISHING JOURNAL OF PHYSICS: CONDENSED MATTER

J. Phys.: Condens. Matter **19** (2007) 106203 (8pp) doi:10.1088/0953-8984/19/10/106203

Ferromagnetism and infrared conductivity of the homogeneous hexaboride alloy $Eu_{1-x}Ca_xB_6$

Jungho Kim[1], SungHoon Jung[2], J H Noh[2], B K Cho[3] and E J Choi[2,4]

[1] Department of Physics, University of Toronto, Toronto, ON, M5S 1A7, Canada
[2] Department of Physics and BK21 Core Program, University of Seoul, Seoul 130-743, Republic of Korea
[3] Center for Frontier Materials and Department of Materials Science and Engineering, K-JIST, Gwangju 500-712, Korea

E-mail: echoi@uos.ac.kr

Received 5 October 2006, in final form 24 January 2007
Published 15 February 2007
Online at stacks.iop.org/JPhysCM/19/106203

Abstract

We have studied the magnetic and optical properties of hexaboride $Eu_{1-x}Ca_xB_6$ for $x = 0$, 0.13, 0.25, 0.35, 0.54 and 1.0 from measurements of dc magnetization and wide-range absolute reflectivity. The ferromagnetic transition temperature T_c decreases with Ca-doping and is completely suppressed when x exceeds 0.35. The Drude plasma frequency ω_p^2 also decreases with x and disappears at the same composition. We have analysed this correlation between T_c and ω_p^2 in terms of the RKKY theory. We have also simulated optical spectra of $Eu_{1-x}Ca_xB_6$ using the effective medium theory and compare them with the measured data. The results show that $Eu_{1-x}Ca_xB_6$ is not a composite of EuB_6 and CaB_6 but forms a homogeneous magnetic alloy.

1. Introduction

The rare-earth hexaboride compound EuB_6 has a long history as a prototypical metallic ferromagnet [1]. The crystal structure is rather simple, where the Eu^{2+} ion and B_6 octahedra form a cubic unit cell. The dc resistivity shows metallic temperature dependence due to low density ($\sim 10^{19}$ cm^{-3}) carriers [1–3]. The Eu^{2+} ions ($S = 7/2$) order ferromagnetically at $T_c \sim 15$ K [4, 5]. The ferromagnetism (FM) is closely related with conducting carriers, as manifested by the large drop of resistivity at $T < T_c$ [1], the change of resistivity with magnetic field [2], and the significant blue shift of the reflectivity plasma edge below T_c [6]. Also T_c is enhanced with external pressure, which Cooley *et al* interpreted in terms of the Ruderman–Kittel–Kasuya–Yosida (RKKY) mechanism with Eu^{2+} moments and the free carriers [7]. Although the band structure of EuB_6 is controversial, recent theoretical calculation and experiments support a semi-metallic band overlap at the X point of Brillouin zone [8–13].

[4] Author to whom any correspondence should be addressed.

Exchange interaction between these carriers and the local Eu 4f moment can lead to the carrier mediated ferromagnetism of EuB_6 [7].

When Eu is replaced by Ca, both the metallic and magnetic behaviours of EuB_6 are significantly changed [14–17]. In $Eu_{1-x}Ca_xB_6$, the Eu ions form a random magnetic lattice due to the incorporation of non-magnetic Ca. One expects that the bulk T_c will be changed as a result. Also the carrier density varies greatly, because although Ca is isovalent with Eu ($= +2$), the semimetal band overlap can be affected by the substitution as discussed in [17]. We will measure the changes of the two quantities with x and examine a possible correlation between them. This will allow us to understand how the ferromagnetic transition depends on the charge density in this EuB_6 based magnetic alloy.

In recent years, ferromagnetism in dilute magnetic semiconductors (DMSs) has been studied intensively due to their potential application in new spin electronics devices. In DMS, the magnetic ions are randomly incorporated into a semiconductor (such as Mn in $Ga_{1-x}Mn_xAs$) and they couple with charges in the host semiconductor through exchange interaction [18]. This can lead to bulk ferromagnetism and spin polarized conduction. There have been claims that T_c at room temperature or even higher can be obtained experimentally [19, 20]. The primary parameters that determine T_c in such systems are the concentration of magnetic ions, carrier density and the exchange coupling constant. In $Eu_{1-x}Ca_xB_6$, Eu concentration and change in carrier density with x provide a chance to study this issue.

2. Experiment

The single-crystal samples were synthesized by a boro-thermal method as described in detail elsewhere [15, 16]. To determine the Eu content x, we measured the dc magnetization $M(H)$ of each sample until it saturates at high magnetic field H. The saturation value is proportional to x, from which we find $x = 0$, 0.13, 0.25, 0.35, 0.54 and 1.0. To measure the magnetization, we used a needle shaped crystal and a field was applied along the direction of the crystal to minimize the demagnetization field. The magnetization measurements were performed using a superconducting quantum interference device magnetometer. For the present optical study, crystals from the same sample batches were used. The reflectance $R(\omega)$ at a near-normal angle of incidence was measured at 300 K in the 20–5000 cm^{-1} and 5000–50 000 cm^{-1} ranges using a Fourier transform spectrometer with an *in situ* overcoating technique [21], and a grating spectrometer with a V–W method, respectively. The crystals were wedged by 2° to avoid internal interference effect.

3. Data and result

Figure 1 shows $M(T)$ of $Eu_{1-x}Ca_xB_6$ measured at an external field $H = 100$ Oe for $T \leqslant 20$ K. In figure 1(a), samples with $x = 0$, 0.13 and 0.25 show a ferromagnetic transition at low temperature. The Curie temperature is about 14.2 K at $x = 0$ if T_c is taken from the inflection point of the transition. As Ca is incorporated, T_c shifts substantially to lower temperature. With a further increase of x to 0.35 (figure 1(b)), the FM disappears and $M(T)$ shows a cusp at ~5 K, indicating an antiferromagnetic (AFM) transition [16]. The cusp of $M(T)$ shifts to lower T at $x = 0.54$.

In figure 2, we present optical reflectivity and conductivity spectra of $Eu_{1-x}Ca_xB_6$. Figure 2(a) shows reflectivity $R(\omega)$ over the wide energy range from far-infrared to ultraviolet frequency taken at room temperature. The high level of $R(\omega)$ at low energy ($\omega < 1200$ cm^{-1} at $x = 0$) shows the metallic response of the compounds. As x increases, the plasma edge shifts

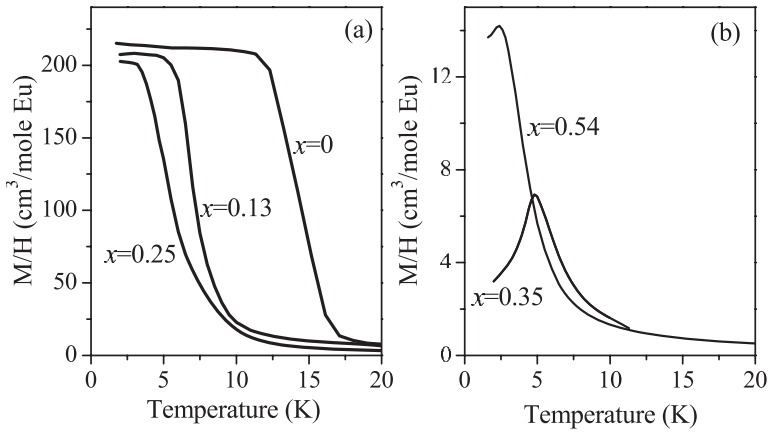

Figure 1. Dc magnetization $M(T)$ of $Eu_{1-x}Ca_xB_6$. (a) Ferromagnetic transition at $x = 0$, 0.13 and 0.25 and (b) $M(T)$ for $x = 0.35$ and 0.54. Data were measured at an applied field $H = 100$ Oe in temperature warming mode.

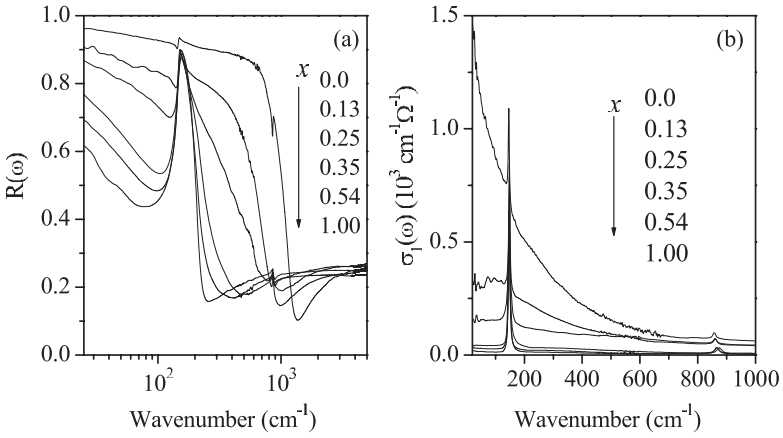

Figure 2. (a) Optical reflectivity of $Eu_{1-x}Ca_xB_6$ ($0 < x < 1$) for a wide frequency range 20 meV $< \omega <$ 1 eV at $T = 300$ K. (b) Drude absorption in optical conductivity in the far-infrared region.

to lower energy and the $R(\omega)$ level decreases. Both observations indicate that the metallicity is suppressed with the Ca-doping. At $x = 0.35$ and 0.54, $R(\omega)$ shows behaviour typical of insulating dielectric solids. The prominent peak at 200 cm^{-1} represents an optical phonon mode. In figure 2(b), optical conductivity, $\sigma_1(\omega)$, which is obtained from the Kramers–Kronig transformation of $R(\omega)$ [17] is shown in the low frequency region. The sharp rise of $\sigma_1(\omega)$ as $\omega \to 0$ corresponds to the Drude conductivity of free carriers. The Drude spectral weight represents the number density of the metallic carrier. As x increases, the Drude conductivity decreases. At $x > 0.35$, it is suppressed completely, which is consistent with the insulating behaviour of dc resistivity[5].

In figure 3, we plot the observed changes of T_c and the squared plasma frequency ω_p^2 together. We estimated ω_p^2 by integrating the Drude conductivity, $\omega_p^2 = 120/\pi \int_0^{\omega_c} \sigma_1(\omega)\, d\omega$,

[5] The weak conductivity at far-infrared range is perhaps due to residual impurities in the samples.

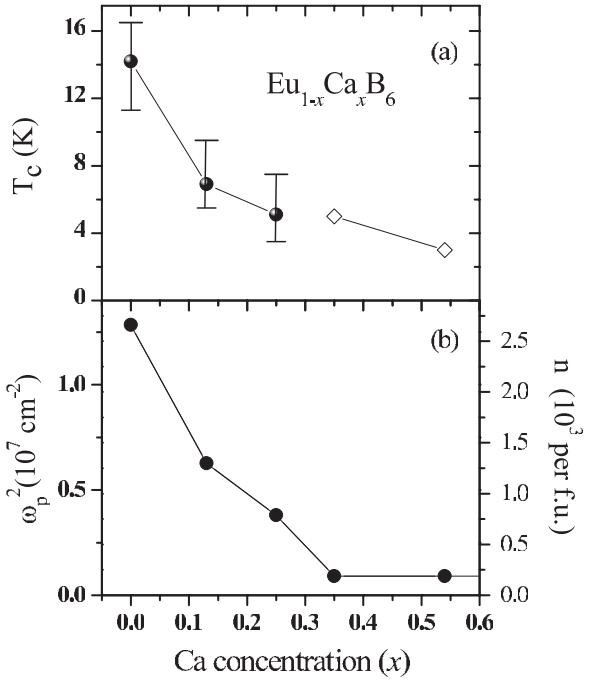

Figure 3. (a) Ferromagnetic transition temperature of $Eu_{1-x}Ca_xB_6$ ($x = 0, 0.13, 0.25, 0.35, 0.54$). For $x = 0.35$ and 0.54, the symbols ($\diamond$) indicate the kink of $M(T)$ in figure 1(a). (b) Squared plasma frequency ω_p^2 obtained from $R(\omega)$ (see the text). ω_p^2 is converted into carrier density on the right vertical axis.

where the cut-off frequency ω_c for the integration was taken as 2000 cm^{-1}. The phonon contribution was subtracted from the sum. ω_p^2 is given as $\omega_p^2 = 4\pi ne^2/m^*$ where n and m^* are the carrier density and the effective mass, respectively. The band structure calculation value of m^* is 0.25 [12]. We take this value of m^* to extract n from ω_p^2 for EuB_6 and also for Ca-doped $Eu_{1-x}Ca_xB_6$ assuming that m^* does not change drastically. The n is shown on the right vertical axis of figure 3(b). As T_c is reduced, n also decreases. When the density is completely suppressed at $x = 0.35$, the magnetic phase shows the crossover from the FM to the AFM state. This result shows clearly that the FM in $Eu_{1-x}Ca_xB_6$ is correlated with the carrier density.

4. Analysis

4.1. RKKY analysis

The correlation between T_c and n shows that the ferromagnetism is mediated by the free carrier. In RKKY theory, T_c is given by [7]

$$T_c = -3\pi \frac{n^2 J^2}{k_B E_F} S(S+1) \sum_i F(2k_F r_i). \tag{1}$$

Here n, k_F ($=3\pi^2 n$) and E_F ($=\hbar^2 k_F^2/2m^*$) represent the free carrier density, the Fermi wavevector and the Fermi energy, respectively. J is the local exchange energy between the magnetic moment and free carrier. $S = 7/2$ is the Eu^{2+} spin and r_i is the distance to the magnetic ion on the ith site. $F(x)$ is the oscillatory RKKY function, $F(x) = (x\cos x - \sin x)/x^4$. In $Eu_{1-x}Ca_xB_6$, the non-magnetic Ca does not contribute to $F(x)$ and the $F(x)$

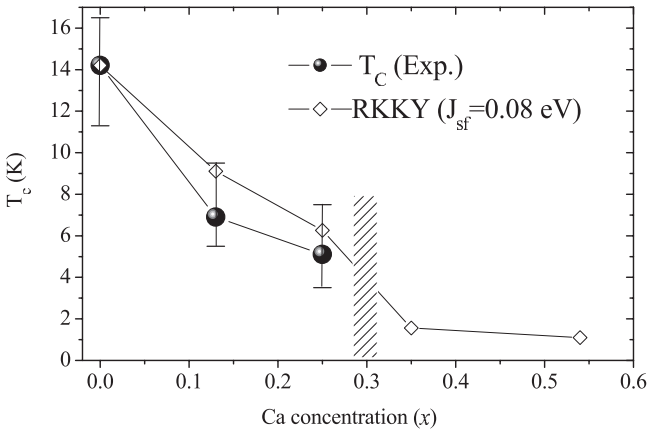

Figure 4. Comparison of experimental T_c with theoretical RKKY results of $Eu_{1-x}Ca_xB_6$. The shaded region represents the crossover from FM to AFM.

summation include only the Eu ions. To calculate T_c, we developed a computing algorithm to simulate the random Eu/Ca occupation of $Eu_{1-x}Ca_xB_6$ and performed the summation of $F(x)$ over only the Eu sites. We used the measured n of figure 3(b) in equation (1). J is a fitting parameter to be determined.

In figure 4, we compare the calculation result of T_c with the measured data. T_c is taken from the inflection point of the transition[6]. The RKKY T_c shows a reasonable agreement with the data when $J = 0.08$ eV was used. This value of J is consistent with 0.1 eV from the homogeneous s–f model calculation by Korenblit [22]. The decrease of T_c with x comes from two sources, the reduction of n and the decrease of Eu ion number. In an earlier paper, we studied the origin of the n change in $Eu_{1-x}Ca_xB_6$ with increasing x [17]. There, it was shown that optical spectra of intra-band and inter-band transitions support the semi-metallic band structure of EuB_6 where the conduction band and valence band overlap with each other. The effect of Ca-doping was that the two electronic bands are modified in a direction where the overlap decreases, in proportion with x, which results in the decrease in carrier density. At $x > 0.35$, the bands are separated from each other and the compound becomes insulating. This is consistent with the insulating behaviour of the measured dc resistivity at $x > 0.35$. In this regime, the RKKY mechanism breaks down. Here the primary magnetic interaction is perhaps the superexchange interaction among Eu 4f electrons which is antiferromagnetic. Such a state can show the observed AFM behaviour at low T.

4.2. Effective medium analysis

In a binary alloy, the two constitutes often show a phase segregation rather than an ideal homogeneous solid solution, where micro-grains of them coexist as a random composite. In $Eu_{1-x}Ca_xB_6$, the RKKY analysis we employed assumed that Eu and Ca occupy the R ion site of the RB_6 unit cell at an atomic scale. If, instead, the two phases EuB_6 and CaB_6 were segregated in small grains, the bulk T_c will be determined mostly by the grain size and density of EuB_6. It is thus necessary to check the micro-structure of $Eu_{1-x}Ca_xB_6$. Tools such as electron or x-ray microscopy can probe directly the Eu/Ca distribution but as an alternative method we can utilize our optical conductivity data to study this issue. If $Eu_{1-x}Ca_xB_6$ is a random composite of

[6] The magnetic transition occurs in the broad temperature range and the error bar is used to show this range.

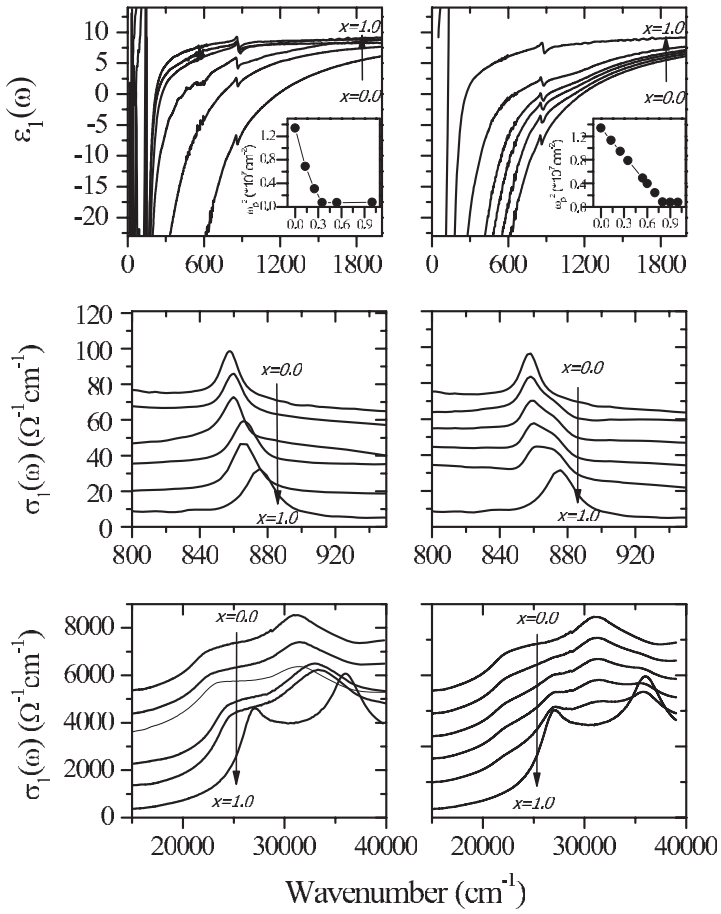

Figure 5. Comparison of the experimental optical spectra of $Eu_{1-x}Ca_xB_6$ with predictions of the effective medium theory. Top panel: Drude dielectric constant $\varepsilon_1(\omega)$. The inset shows the plasma frequency obtained from the zero crossing $\varepsilon_1(\omega_p) = 0$. Middle panel: optical conductivity of the infrared phonon peak in the far-infrared region. Bottom panel: interband transition spectrum in the ultraviolet region.

a EuB_6 grain and a CaB_6 grain, the complex dielectric constant $\epsilon(\omega)$ measured from experiment is given by the effective medium approximation (EMA) as

$$(1-f)\frac{\varepsilon_a-\varepsilon}{\varepsilon_a+2\varepsilon}+f\frac{\varepsilon_b-\varepsilon}{\varepsilon_b+2\varepsilon}=0. \tag{2}$$

Here $\epsilon_a(\omega)$ and $\epsilon_b(\omega)$ represent the dielectric constant of EuB_6 and CaB_6, respectively, and f is the volume fraction of CaB_6 ($=x$). This relation holds when the wavelength of the incident light is much larger than the size of the assumed grains. Using equation (2), we construct the effective $\epsilon(\omega)$ using the measured $\epsilon_a(\omega)$ and $\epsilon_b(\omega)$. In figure 5, the calculation results are compared with the measured $\epsilon(\omega)$ spectra of $Eu_{1-x}Ca_xB_6$ in three different energy regions. In the top panel, we plot the real part $\epsilon_1(\omega)$ in the low energy range. As ω decreases, $\epsilon_1(\omega)$ changes sign and increases (negatively) rapidly which reflects the Drude carrier response. From the zero crossing of $\epsilon(\omega)$, we obtain the (screened) plasma frequency ω_p, $\varepsilon_1(\omega_p) = 0$. Note that in both figures, ω_p decreases as Eu is replaced with Ca and eventually becomes insulating. However, in the EMA result, the metal to insulator transition occurs at $x = 0.7$ ($=2/3$) which

does not agree with $x = 0.35$ in the experiment. The middle panel shows an infrared phonon peak in the FIR region. This mode is considered to come from the B_6 internal vibration. The peak frequency is about 860 and 875 cm^{-1} for EuB_6 and CaB_6, respectively. In the region of intermediate x, the peak structure of EMA is clearly different from experiment: in the EMA result, the spectrum consists of two peaks which can be considered as a superposition of the peaks in EuB_6 and CaB_6 weighted by their compositions. In contrast, the experimental curve shows a single peak shifting gradually from $x = 0$ to 1. This behaviour shows that the unit cell is homogeneous over the entire crystal volume in $Eu_{1-x}Ca_xB_6$ denying two lattice parameters by EuB_6 and CaB_6 composites.

Similar behaviour is seen in the ultraviolet frequency range in the bottom panel. The two peaks at 20 000 $cm^{-1} < \omega < 40\,000$ cm^{-1} represent the interband transition from the valence band to the conduction band. The excitation frequencies are different in EuB_6 and CaB_6 because the band energies are different as we discussed in [17]. In EMA, the peak structure is again a weighted superposition of $x = 0$ and 1, whereas in experiment, each peak shifts, preserving the two-peak structure. These observations of the plasma frequency, phonon peak and the electronic interband transition show unequivocally that the EMA does not explain the optical spectra of our samples. Therefore, it provides evidence that this system is not a phase segregated composite of EuB_6 and CaB_6 clusters but an ideal homogeneous solid alloy. It supports the idea that the magnetic behaviour of $Eu_{1-x}Ca_xB_6$ is driven by a microscopic mechanism such as the RKKY analysis we employed in a previous section. Also this system can be a good model for studying the physics of random magnetic alloys, which is the subject of intense interest in recent DMS research.

5. Summary

We have shown that the T_c change in $Eu_{1-x}Ca_xB_6$ is correlated with the ω_p^2 change. This correlation between T_c and ω_p^2 is understood in terms of the RKKY interaction. Also, from the simulation of optical spectra of $Eu_{1-x}Ca_xB_6$ using the EMA and comparison with the measured data, we find that our $Eu_{1-x}Ca_xB_6$ sample is not a composite of EuB_6 and CaB_6 but forms a homogeneous magnetic alloy.

Acknowledgments

We thank C C Homes for help in the optical spectroscopic measurement. This work was supported by a KRF Grant no. 2002-070-C00044 and the KOSEF through CSCMR.

References

[1] Guy C N, von Molnar S, Etourneau J and Fisk Z 1980 *Solid State Commun.* **33** 1055
[2] Süllow S, Prasad I, Aronson M C, Bogdanovich S, Sarrao J L and Fisk Z 2000 *Phys. Rev.* B **62** 11626
[3] Wigger G A, Monnier R, Ott H R, Young D P and Fisk Z 2004 *Phys. Rev.* B **69** 125118
[4] Matthias B T, Geballe T H, Andres K, Corenzwit E, Hull G W and Maita J P 1968 *Science* **159** 530
[5] Kasaya M, Tarascon J M, Etourneau J and Hagenmuller P 1978 *Mater. Res. Bull.* **13** 1055
[6] Degiorgi L, Felder E, Ott H R, Sarrao J L and Fisk Z 1997 *Phys. Rev. Lett.* **79** 5134
[7] Cooley J C, Aronson M C, Sarrao J L and Fisk Z 1997 *Phys. Rev.* B **56** 14541
[8] Goodrich R G, Harrison N, Vuillemin J J, Teklu A, Hall D W, Fisk Z, Young D and Sarrao J 1998 *Phys. Rev.* B **58** 14896
[9] Aronson M C, Sarrao J L, Fisk Z, Whitton M and Brandt B L 1999 *Phys. Rev.* B **59** 4720
[10] Terashima T, Terakura C, Umeda Y, Kimura N, Aoki H and Kunii S 2000 *J. Phys. Soc. Japan* **69** 2423
[11] Hall D, Young D P, Fisk Z, Murphy T P, Palm E C, Teklu A and Goodrich R G 2001 *Phys. Rev.* B **64** 233105

[12] Massidda S, Continenza A, Pascale T M D and Monnier R 1997 *Z. Phys.* B **102** 83
[13] Kuneš J and Pickett W E 2004 *Phys. Rev.* B **69** 165111
[14] Paschen S, Pushin D, Schlatter M, Vonlanthen P, Ott H R, Young D P and Fisk Z 2000 *Phys. Rev.* B **61** 4174
[15] Rhyee J-S, Cho B K and Ri H-C 2003 *Phys. Rev.* B **67** 125102
[16] Rhyee J-S, Oh B H, Cho B K, Kim H C and Jung M H 2003 *Phys. Rev.* B **67** 212407
[17] Kim J-H, Lee Y, Homes C C, Rhyee J-S, Cho B K, Oh S-J and Choi E J 2005 *Phys. Rev.* B **71** 075105
[18] Wolf S A, Awschalom D D, Buhrman R A, Daughton J M, von Molnár S, Roukes M L, Chtchelkanova A Y and Treger D M 2001 *Science* **294** 1488
[19] Saito H, Zayets V, Yamagata S and Ando K 2003 *Phys. Rev. Lett.* **90** 207202
[20] Macdonald A H, Schiffer P and Samarth N 2005 *Nat. Mater.* **4** 195
[21] Homes C C, Reedyk M, Crandles D A and Timusk T 1993 *Appl. Opt.* **32** 2976
[22] Korenblit I Y 2001 *Phys. Rev.* B **64** 100405